Growth of Carbon Particles during Detonation of Condensed Explosives

A. P. Ershov^{a,*}

^a Lavrentyev Institute of Hydrodynamics, Siberian Branch, Russian Academy of Sciences, Novosibirsk, 630090 Russia *e-mail: ers@hydro.nsc.ru

Received April 3, 2024; revised May 15, 2024; accepted May 15, 2024

Abstract—The growth of particles behind the detonation wave front in condensed explosives is considered based on the physical estimates and experimental results obtained in recent years. The focus is on the large difference in particle size due to the presence or absence of hydrogen in the explosive.

Keywords: detonation, explosion, carbon, coagulation

DOI: 10.1134/S0010508225700078

INTRODUCTION

The detonation of most explosives leads to the release of excess carbon. This phenomenon was for a long time considered an acceptable drawback of explosive technologies and did not attract particular attention. Some exception was considerations of the contribution of carbon to the energy release. The relatively slow process of carbon condensation was assumed to exhibit the non-ideality effects observed in substances with a significantly negative oxygen balance [1, 2]. These works suggested unlimited particle clustering, resulting in a prolonged energy release.

The discovery of the detonation synthesis of diamond has rekindled interest in the release of free carbon in an explosion. The synthesis of diamond from the carbon of an explosive was first discovered at RFNC-VNIITF (Snezhinsk) by Volkov, Danilenko, and Elin in 1963 [3]. This striking result did not become widely known for a number of reasons outlined in [4].

In 1982, detonation synthesis was discovered again at the Institute of Hydrodynamics of the Siberian Branch of the USSR Academy of Sciences by Staver, Lyamkin, and Petrov. Preliminary results (in a somewhat roundabout presentation) are reported in [5, 6]. In subsequent years, a significant amount of research was conducted at the Institute of Hydrodynamics and a number of other organizations. Pilot industrial production was reported already in the 1988 publication [7]. Ultradispersed diamond formed from the carbon of explosives was so different from both natural and artificial diamonds obtained by other methods that it could claim to be a new carbon modification [6].

After the appearance of key publications [7, 8], the carbon material collected after explosions was studied in many laboratories around the world. The results were in sharp contrast to the picture of unlimited growth described in [1]: the typical particle size was several nanometers.

Estimates of the growth kinetics showed that Brownian coagulation should lead to much larger sizes (tens of nanometers). Naturally, the idea arose that the particle growth is limited due to the exit from the conditionally liquid state with increasing particle size [9-11].

However, the explosion products of the hydrogen-free explosive benzotrifuroxan (BTF) have been found to contain particles of hundreds of nanometers in size [12] obviously not subject to size limitations. For such particles, Brownian coagulation turned out to be too slow. Mal'kov [13] pointed out the importance of microturbulence (or shear flows) that occur in detonations products due to material heterogeneity and are capable of dramatically accelerating coagulation: a particle size of 200 nm can be achieved in a time of about 3 μ s.

Later, data on real-time particle growth dynamics were obtained by small-angle synchrotron X-ray scattering [14–18]. This allows growth model predictions to be compared with experiment. Such a comparison is made in this paper. The processes influencing the formation and growth of particles are discussed.

BROWNIAN COAGULATION

The release of free carbon during detonation occurs mainly in the chemical reaction zone. Carbon is released in the form of atoms or small clusters which combine into nanometer-sized, and possibly larger, particles. Experiments, within their resolution, have confirmed the formation of particles of a few nanometers in size within fractions of a microsecond. Further growth can last for microseconds until expansion of the material begins to have an effect. It is natural to assume that in the case of extreme and rapid supersaturation, the main growth mechanism is coagulation [1, 9, 10]. Recently, more sophisticated theories have been developed, e.g., [19], which consider the fragmentation of particles and their ripening by exchanging fragments, but in view of the uncertainties involved, such models seem overcomplicated. In this and the following sections, we discuss simplified approaches that can be used to conduct a comparison between theory and experiment within the available accuracy.

The coagulation process is described by the Smoluchowski equations [20]:

$$\frac{dn(m)}{dt} = \frac{1}{2} \sum_{i+j=m} K(i,j) n(i) n(j) - n(m) \sum_{j=1}^{\infty} K(m,j) n(j).$$
 (1)

Here t is time, n(m) is the concentration of particles containing m monomers (for brevity, we will speak of particles of mass m, considering the mass of the monomer, in our case, a carbon atom, to be the unit mass), and K(i, j) is the coagulation kernel describing the rate of coagulation of particles of masses i, j in a unit volume. The first term on the right side of Eq. (1) describes the formation of particles of mass m from clusters of smaller masses, and the second term describes the elimination of these particles upon contact with any others.

Summing all Eqs. (1), we obtain the rate of change of the total concentration $N = \sum_{m} n(m)$:

$$\frac{dN}{dt} = -\frac{1}{2} \sum_{i,j=1}^{\infty} K(i,j) n(i) n(j). \tag{2}$$

The evolution of the distribution n(m) depends significantly on the type of coagulation kernel. In the simplest case where K(i, j) = K = const under the initial conditions $n(1) = n_0$ and n(m > 1) = 0, the analytical solution of Eqs. (1) is known [20, 21]. In particular, the equation for N is greatly simplified:

$$\frac{dN}{dt} = -\frac{K}{2}N^2. (3)$$

From (3) we have

$$N = \frac{n_0}{1 + n_0 K t / 2},\tag{4}$$

where n_0 is the initial concentration of monomers.

For Brownian coagulation, the condition K(i, j) = const is quite a reasonable approximation. In the case of viscous particle motion,

$$K(i,j) = 4\pi(D_i + D_j)(r_i + r_j) = \frac{2kT}{3\mu} \frac{(r_i + r_j)^2}{r_i r_j} = \frac{2kT}{3\mu} \frac{(i^{1/3} + j^{1/3})^2}{i^{1/3} j^{1/3}},$$
 (5)

where D_i and D_j are the diffusion coefficients of particles of species i and j, r_i and r_j are their radii, k is Boltzmann's constant, T is the temperature, and μ is the viscosity of the medium. The kernel K(i, j) takes a minimum value when i = j:

$$K(i,i) = \frac{8kT}{3\mu}.$$

The dependence of (5) on the ratio i/j normalized to the minimum value is shown in Fig. 1 (curve B). This flat minimum can be taken in the first approximation as an estimate of K. Then Eq. (4) leads to

$$N = \frac{n_0}{1 + \frac{4n_0kT}{3\mu}t}.$$
 (6)

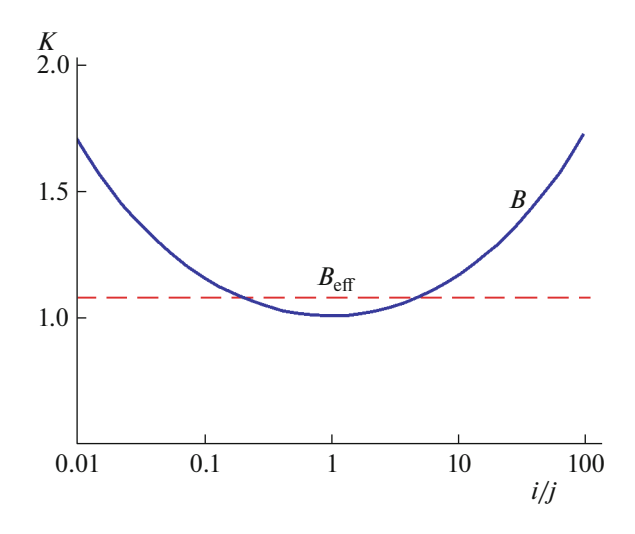


Fig. 1. Brownian coagulation kernel vs. relative particle mass.

A convenient variable for estimating the growth rate is the average number of monomers in a particle $M = n_0/N$. In the same approximation, we obtain

$$\frac{dM}{dt} = \frac{4kTn_0}{3u}. (7)$$

As can be seen, for the case of a constant kernel, the value of M increases linearly with time.

Since with a marked difference between the particles, the coagulation kernel K(i, j) increases, the total concentration N according to (2) decreases faster and the estimate (7) will be somewhat underestimated. Numerical calculations [22, 23] have shown that over time a self-similar distribution develops and the average mass increases as

$$\frac{dM}{dt} = \frac{4\beta k T n_0}{3u};$$

i.e., it differs from (7) in the coefficient β close to unity (1.08 according to [22] and 1.064 according to [23]). The dashed line $B_{\rm eff}$ in Fig. 1 shows the effective level of K for Brownian coagulation. Taking this weak effect into account in approximate estimates seems unnecessary.

Thus, Brownian coagulation is described by the equation

$$\frac{dM}{dt} = \frac{1}{\tau_B},\tag{8}$$

where the characteristic Brownian time is $\tau_B = 3\mu/4kTn_0 = 3\mu/4kT\phi n_C$. Here ϕ is the volume fraction of the condensed phase and n_C is the concentration of carbon atoms in the particles.

Under conditions corresponding to the Chapman–Jouguet state for dense explosives (\approx 30 GPa, \approx 4000 K), the following values for the viscosity of detonation products μ were proposed: 0.01 g/(cm s) [1]; \approx 0.01 g/(cm s) (for the gas phase [24]); \approx 0.02 g/(cm s) [25, 26]. We use as some average the value $\mu = 0.014$ g/(cm s), which slightly exceeds the viscosity of water under normal conditions.

The concentration of free carbon atoms under the same conditions was estimated at 10^{22} cm⁻³ for HMX [1] and at 3×10^{22} cm⁻³ for TATB [26]. In experimental studies [27, 28], the yield of solid carbon was approximately 0.5×10^{22} cm⁻³ for HMX, 10^{22} cm⁻³ for BTF, and 2×10^{22} cm⁻³ for TNT. The latter value is in good agreement with measurements [29]. For comparison of the sizes of particles obtained during detonation of BTF and TNT/RDX mixtures (commonly used to synthesize nanodiamonds), we use the average value $n_0 = 10^{22}$ cm⁻³. Almost all released carbon is in the form of small particles; at this concentration, their volume fraction is $\phi \approx 0.05$.

Then at a temperature $T \approx 4000$ K, the time $\tau_B \approx 2 \times 10^{-12}$ s. It should be noted that this estimate may contain an error of a factor of 2 to 3 due to the uncertainty of the values of the viscosity and concentration n_0 .

As noted in [30], for ϕ of the order of several percent, a noticeable acceleration of coagulation should be expected, since the gaps between particles become approximately equal to the diameters of the particles. On the other hand, there may be a slowdown of Brownian growth by the gas medium. Gas molecules that adhere to the surface of carbon particles are capable of slowing down the coagulation process. These effects compensate each other at least partially. Therefore, we will accept the above estimate.

According to (8), at $\tau_B \approx 2 \times 10^{-12}$ s already after 2 µs, it should be expected that the average number of atoms in a particle M will reach 10^6 , which corresponds to a diameter of more than 20 nm. Meanwhile, under typical synthesis conditions, the particles recovered after the explosion are much smaller. The characteristic size of ultrafine detonation diamonds is usually 4–7 nm [7, 8]. A particle with a diameter of 5.5 nm contains about 15000 carbon atoms, which is almost two orders of magnitude smaller than the expected quantity.

In [9, 10] this discrepancy is explained by the slowdown of coagulation with increasing particle size. At temperatures below the melting point of a massive sample, small particles still behave like liquid drops and coagulate upon contact, but after reaching a larger size, they are transformed into a solid state. Naturally, this transition is not abrupt, and the coagulation of large particles may continue due to fluctuations, although at a lower probability. The growth of compact particles can also continue due to the adhesion of small particles to large ones, but over time the particle size distribution freezes. Similar considerations are developed in [11].

Contact of large solid particles may lead to a continuation of aggregation, in which particles stick together without mixing, largely retaining their shape and individuality. At this stage, sparse (fractal) aggregates are formed that can be observed in recovered explosion products [9, 10, 31]. The picture described above was qualitatively confirmed by molecular dynamics simulation in a primitive two-dimensional formulation [32, 33]. Later, the results of detailed three-dimensional calculations were published [26], which also demonstrated the transition from coagulation to aggregation. From the above data, it can be concluded that for typical conditions behind the detonation front, large particles are those containing much more than 1000 atoms (diameter greater than 2 nm). In [34], protrusions on the surface of large particles are demonstrated that can be interpreted as the result of adhesion and partial spreading of small clusters.

COAGULATION IN TURBULENT AND SHEAR FLOW

Abnormally large diamond particles 100–1000 nm in size were found [12] in the detonation products of BTF. The size of coherent scattering regions was about 30 nm, much larger than in the synthesis using conventional explosives, e.g., mixtures of TNT and RDX. Presumably, the increased size was due to the high temperature developed during the explosion of BTF, so that particle coagulation occurred in the liquid phase of carbon under stability conditions.

However, as the above estimates show, particles hundreds of nanometers in size do not have time to form due to diffusion. Whereas for particles a few nanometers in size, Brownian coagulation seemed too rapid, in the case of BTF, its rate is obviously insufficient.

An explanation for such rapid growth was proposed in [13]. During detonation of solid explosives, their heterogeneous structure should be expected to lead to the occurrence of microscopic flows on scales of the order of the explosive grain size (microturbulence). These flows can significantly accelerate the mutual approach of particles. The possibility of accelerating coagulation due to shear flow is also mentioned in [13]. For both of these variants, the coagulation kernel can be written as follows [20, 35, 36]:

$$K(i,j) = A(i^{1/3} + j^{1/3})^3. (9)$$

The similarity in the structure of the kernels reflects the contribution of the convective transport of particles; in this case, the factor A is determined by the type of process. Based on formula (9), the rate of coagulation is proportional to the masses of the particles. Therefore, the increase in the average mass with time is exponential rather than linear as in the case of Brownian coagulation.

Analytical solutions are known for the coagulation equations for a simplified kernel of the form K(i, j) = A(i + j) [37–39]. In this case, Eq. (2) leads to the following dynamics of the total concentration:

$$\frac{dN}{dt} = -\frac{A}{2} \sum_{i,j=1}^{\infty} (i+j)n(i)n(j) = -A \sum_{i,j=1}^{\infty} in(i)n(j) = -An_0N.$$
 (10)

It can be seen that N decreases exponentially, and the average mass of particles defined as $\overline{M} = n_0/N$ increases exponentially with time:

$$\overline{M} = \exp(An_0t). \tag{11}$$

However, expression (11) somewhat underestimates the actual rate of particle growth. The particle mass distribution function has the following form [37, 38]:

$$n(m) \propto \exp(-An_0t)m^{-3/2} \exp\left(-\left(1 - \sqrt{1 - \exp(-An_0t)}\right)^2 m\right).$$
 (12)

For large values of An_0t , the second exponent on the right side is simplified to $\exp(-m\exp(-2An_0t)/4)$. This factor truncates the power-law decay at the mass $m_* \sim \exp(2An_0t)$. It is evident from (12) that the main contribution to the total concentration N is due to small particles, whereas the total mass is determined by large particles at the right edge of the distribution. Therefore, the best idea of the characteristic particle mass is afforded by the median mass (for in which half of the total mass is made up of smaller particles, and the other half of larger ones). Keeping the notation M for this median mass, we have

$$M \cong \exp(2An_0t). \tag{13}$$

Next, we estimate the characteristic time of particle growth. These times for (11) and (13) differ by a factor of two, so that the difference between them is insignificant for our order-of-magnitude estimates. In Brownian coagulation, there is no sharp increase in the distribution function in the region of small sizes, the average and median masses are close and it is much less needed to distinguish between them.

Note that the kernel (9) can be represented as

$$K(i,j) = A(i+j)F(i,j),$$

$$F(i,j) = 1 + 3\frac{i^{2/3}j^{1/3} + i^{1/3}j^{2/3}}{i+j}.$$

The function F(i, j) depends only on the ratio i/j. This dependence is shown in Fig. 2 (curve S). The value of F(i/j) is always greater than 1 and reaches a maximum of 4 at i = j. Therefore, the particle growth is faster for the real kernel (9) than for the simplified kernel according to formula (13). As follows from the numerical solution obtained in [40], the coefficient 2 in (13) should be replaced by 6.41 (acceleration by a factor of ≈ 3.2). The dashed line $S_{\rm eff}$ in Fig. 2 indicates the effective average value of F (3.2 of the minimum value achieved when the difference between particles is large). Therefore, the particle growth in the shear or turbulent regime is described by the equation

$$\frac{dM}{dt} = \frac{M}{\tau_S}, \quad \tau_S = \frac{1}{6.41An_0} = \frac{1}{6.41A\phi n_C},\tag{14}$$

where τ_s is the characteristic growth time.

In particular, if there is developed turbulence behind the detonation front, we can use the result of [35, 36]:

$$K(i,j) = \sqrt{\frac{8\pi\epsilon}{15\nu}} (r_i + r_j)^3, \quad A_T = \frac{0.309}{n_C} \sqrt{\frac{\epsilon}{\nu}}.$$
 (15)

Here ε is the rate of turbulent energy dissipation, v is the kinematic viscosity of the medium, and A_T is the coefficient A for the turbulent regime. According to [13], at a viscosity of 5×10^{-3} cm²/s, an explosive grain size I = 50 μ m, and a relative velocity of adjacent volumes of the medium u = 50 m/s ($\varepsilon \simeq u^3/I$), particles of size 200 nm ($M \approx 8 \times 10^8$) can form in about 3 μ s.

However, there are reasons to doubt the estimates of [13]. If we adopt the data proposed in that paper, the small-scale Reynolds number is Re = ul/v = 5000. This value does not seem sufficient for the rapid formation of a well-developed turbulence spectrum. According to the analysis in [41], the minimum

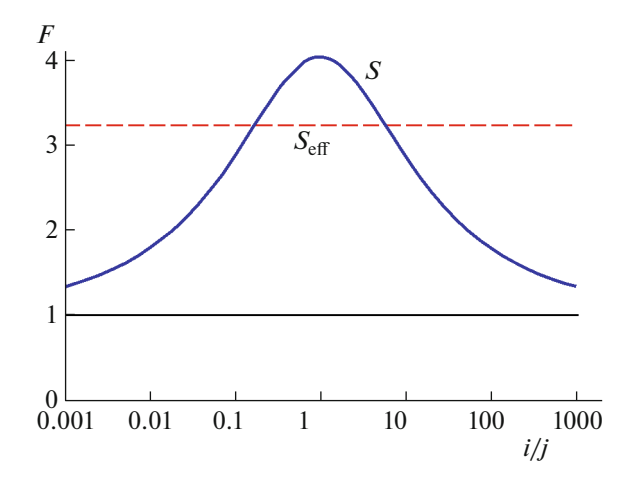


Fig. 2. Function F vs. relative particle mass in shear coagulation.

required Reynolds number should be not less than $(1-2)\times10^4$. Clearly, the parameters adopted in [13] may vary, but even if the Reynolds number reaches the required level, the occurrence of turbulence is not instantaneous but requires a time interval at least severalfold longer than the interaction time of neighboring microvolumes $l/u \cong 1$ µs.

For shear flow, Smoluchowski [20] obtained the expression

$$K(i,j) = \frac{4}{3}\Gamma(r_i + r_j)^3, \quad A_S = \frac{\Gamma}{\pi n_C},$$
 (16)

where A_S is the coefficient A for the shear regime and Γ is the velocity gradient in the transverse direction, e.g., $\frac{\partial v_x}{\partial v}$ for flow in the x direction.

As can be seen from (15) and (16), the rates of the processes differ mainly in the characteristic frequencies included in the coefficients A: for A_T , this is the inverse Kolmogorov time $\sqrt{\varepsilon/v} \approx 7 \times 10^7$ 1/s, and for A_S , the inverse shear time Γ . When using $\Gamma \approx u/l \approx 10^6$ 1/s, the turbulent coagulation rate exceeds the shear rate by a factor of ≈ 70 ; i.e., the influence of shear is insignificant.

However, this estimate is grossly underestimated. It is known that in solid explosives, the post-shock chemical reaction begins at numerous hot spots where the shock heating far exceeds the average level. From these hot spots, combustion waves propagate, and when they merge, the reaction is completed. The reaction time can be estimated as $\tau = \delta/u_B$, where δ is the distance between hot spots and u_B is the combustion wave velocity relative to the material. Due to the chaotic arrangement of hot spots, the flow is also accompanied by shears, with the characteristic velocity gradient Γ being of the order of $u_B/\delta \cong 1/\tau$. BTF, which is mainly discussed in this section, is known as a sensitive explosive with fast reaction. We are not aware of direct dynamic measurements of the reaction time of BTF, but our data on the duration of electrical conductivity peaks behind the detonation front [42] gave a range of 30–40 ns. These results are upper bounds, so that the actual reaction time is most likely shorter. Setting the BTF reaction time equal

to 20 ns, we obtain a gradient $\Gamma \cong 5 \times 10^7$ 1/s, which is similar to the estimate based on the assumption of well-developed microturbulence. At the same time, the shear mechanism seems more physically plausible. However, since the kinetics of turbulent and shear coagulation are formally close, both mechanisms can act together.

In the shear regime, the characteristic growth time is

$$\tau_S = \frac{1}{6.41 A_S n_0} = \frac{\pi}{6.41 \Gamma \phi}.$$

At $\Gamma = 5 \times 10^7$ 1/s and $\phi = 0.05$, the time is $\tau_S \approx 2 \times 10^{-7}$ s.

The decay time of shear flows is of the order of $\delta^2/\nu \cong 20~\mu s$ at $\delta=3~\mu m$ and $\nu=0.005~cm^2/s$. This time is much longer than the time of expansion of detonation products (μs). Below, the viscous decay will be neglected.

COMBINED EFFECT OF DIFFUSION AND SHEAR. INFLUENCE OF EXPANSION

The characteristic times τ_B and τ_S estimated above differ by five orders of magnitude. Therefore, the Brownian and shear coagulation kinetics are sharply different. Under our conditions, the first mechanism leads to rapid initial growth of mass: $M \approx t/\tau_B$, but for long times, this linear growth turns out to be insufficient. The second mechanism provides exponential growth, which, in contrast, will be too slow at the beginning of the process due to the relatively long time τ_S . It is natural to consider the combined action of both mechanisms.

It has been shown [43] that for the combined action of diffusion and shear, the coagulation kernel is somewhat larger than the sum of the corresponding kernels, but this difference (less than 30%) is negligible at our level of accuracy. The summation of the kernels gives exact asymptotics in the extreme cases of dominance of one of the mechanisms. The particle growth is determined by the effective values of the Brownian kernel K (see Fig. 1) and the function F (see Fig. 2) which are close to their extrema. This allows us in a qualitative consideration to sum the right sides of Eqs. (8) and (14). Therefore, it is reasonable to write the growth kinetics as

$$\frac{dM}{dt} = \frac{1}{\tau_B} + \frac{M}{\tau_S},$$

$$\tau_B = \frac{3\mu}{4kTn_0} = \frac{3\mu}{4kTn_C\phi}, \quad \tau_S = \frac{\pi}{6.41\phi\Gamma}.$$
(17)

The rates of mass growth due to the Brownian and shear mechanisms become equal at $M_* = \tau_S/\tau_B \simeq 10^5$, which is achieved in time slightly shorter than $M_*\tau_B$, i.e., in about 0.1 µs. The Brownian mechanism is dominant before this time, and the shear mechanism dominates after this time.

An explosion always leads to a rapid expansion of the medium, which should slow down coagulation. To take this effect into account, Eqs. (1) should be corrected:

$$\frac{dn(m)}{dt} = \frac{1}{2} \sum_{i+j=m} K(i,j) n(i) n(j) - n(m) \sum_{i=1}^{\infty} K(m,j) n(j) - \frac{n(m)}{V} \frac{dV}{dt}.$$
 (18)

Here V(t) is the specific volume of the considered element of the medium. If, at some time, coagulation is turned off, the last term in (18) will provide the particle concentration reduction rate necessary to maintain the number of particles.

We express n(m) in the form

$$n(m) = \frac{V_0}{V} \eta(m). \tag{19}$$

In the new variables $\eta(m)$, the equations take the form

$$\frac{V}{V_0} \frac{d\eta(m)}{dt} = \frac{1}{2} \sum_{i+j=m} K(i,j) \eta(i) \eta(j) - \eta(m) \sum_{j=1}^{\infty} K(m,j) \eta(j).$$
 (20)

Suppose that expansion does not affect the coagulation kernel. It is easy to see that in this case, the evolution of $\eta(m)$ reproduces the evolution of n(m) in the absence of expansion, with the difference that the physical time t is replaced by the scaled time \tilde{t} defined by the formula

$$d\tilde{t} = \frac{V_0}{V} dt.$$

With this correction, all growth rate estimates, including (17), are retained.

The growth will be limited by the function V_0/V . It is common to use cylindrical charges, and in the roughest approximation, the expansion occurs in directions transverse to the axis. For the estimation, we use the expansion law in the form

$$\frac{V}{V_0} = \left(1 + \frac{t}{\tau_H}\right)^2,\tag{21}$$

where the characteristic time of hydrodynamic expansion τ_H is of the order of the ratio of the charge radius R to the speed of sound c. Then

$$\tilde{t} = \frac{t\tau_H}{t + \tau_H}. (22)$$

The time \tilde{t} is always less than t, and in the limit, it reaches the value of τ_H , which is typically a few microseconds. For example, for unlimited Brownian coagulation and $\tau_H \simeq 1 \, \mu s$, the value of M can increase to several millions. The diameter of such particles is $\approx 30 \, \text{nm}$. This again indicates the need (under typical synthesis conditions) to limit the growth at much smaller sizes. For the high-temperature synthesis from BTF, exponential growth by the shear mechanism starts before the particles reach such sizes.

The introduction of the factor V_0/V describes the slowdown of coagulation due to a reduction in particle concentrations. In addition, expansion may affect the coagulation kernel. For the shear mechanism, the effect of expansion on the gradient should primarily be taken into account: $\Gamma = \Gamma_0(V_0/V)^{2/3}$. This follows from the commonly used dependences of pulsation velocities and scales on the density ρ : the velocity is proportional to $\rho^{1/3}$, and the scale changes as $\rho^{-1/3}$ [44].

In addition, expansion distorts the velocity distribution around each particle. Uniform shear is superimposed by radial spreading with the local velocity

$$u \cong \frac{r}{3V} \frac{dV}{dt} \lesssim \frac{2r}{3\tau_H}.$$

The ratio of this velocity to the characteristic shear velocity for the above conditions is

$$\frac{u}{\Gamma r} \simeq \frac{2}{3\Gamma \tau_H} = \frac{2}{3\Gamma \tau_H} \sim 10^{-2},$$

i.e., it can be neglected.

For the Brownian mechanism, the spreading can be more significant. However, Brownian growth is either overlapped with exponential shear (in the case of BTF) or is frozen upon reaching nanometer sizes (for conventional explosives) within fractions of a microsecond. when there is no significant expansion. Therefore, there is no need to consider corrections for spreading. For the same reason, the changes in the quantities μ and T included in τ_B can be neglected.

Thus, from Eq. (17) we move to the following growth model:

$$\frac{V}{V_0} \frac{dM}{dt} = \frac{1}{\tau_B} + \frac{M}{\tau_S} \left(\frac{V_0}{V}\right)^{2/3},$$

$$\tau_B = \frac{3\mu}{4kTn_0} = \frac{3\mu}{4kTn_0\phi}, \quad \tau_S = \frac{\pi}{6.41\phi\Gamma_0}.$$
(23)

Here ϕ is the volume fraction of carbon at the beginning of the process and Γ_0 is the average initial velocity gradient in detonation products. The expansion of detonation products slowing down the growth is taken into account by the factor V/V_0 on left side of (23). The times τ_B and τ_S are considered constant. As before, we assume that for cylindrical charges, the expansion occurs mainly in the radial direction and relation (21) holds.

CALCULATION RESULTS

Since 2000, new synchrotron radiation diagnostics for explosive processes has been developed based on a high-quality X-ray source with extremely low divergence and high pulse repetition rate. In particular, small-angle X-ray scattering (SAXS) enables the first real-time observations of the carbon condensation process [14].

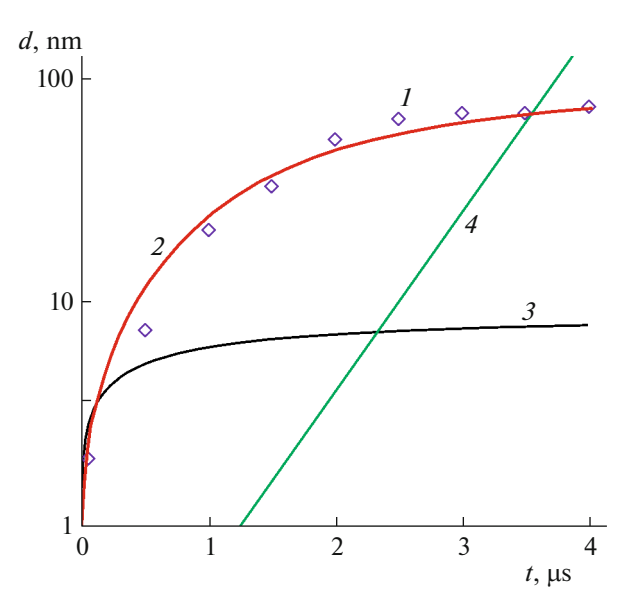


Fig. 3. Comparison of the calculated dynamics of particle sizes in BTF with experiment (the points are the data of [15, 16]).

The intensity of the scattered radiation is proportional to the square of the difference of the densities of particles and their gaseous environment. Since, before the start of expansion, this difference is relatively small, the scattered signal is initially suppressed [45]. Early measurements underestimated this low-contrast effect, which created the impression of carbon condensation lasting for several microseconds. According to later data, the condensation time decreased to $1-2\,\mu s$ [15], with particles of size about 2 nm being detected almost instantaneously (within the resolution of the technique). According to the results of American researchers [17, 18, 34], the time of formation of particles is fractions of a microsecond. This is consistent with the recent Russian data [46] taking into account the formation of sparse aggregates.

Papers [15, 16] containing dynamic SAXS data during detonation of the BTF provide a unique opportunity to compare the growth model (23) with experiment. These papers present the time dependence of particle size for 4 µs during detonation of a cylindrical charge with a diameter of 2 cm. The particle size increases from the initial 2 to 70 nm (Fig. 3). The interpretation of SAXS data is quite difficult, and the results [15, 16] should be considered approximate. However, the difference between the data for BTF and for explosives such as 50/50 TNT/RDX and TATB is quite clearly observed, and the final particle sizes are in good agreement with the microscopic measurements in condensed explosion products.

The comparison was carried out by selecting the characteristic times τ_B , τ_S , and τ_H . For the parallel operation of two processes [Fig. 3, curve 2 corresponding to kinetics (23)], acceptable agreement with experiment can be obtained for $\tau_B = 3 \times 10^{-5} \, \mu s$, $\tau_S = 0.08 \, \mu s$, and $\tau_H = 2 \, \mu s$. The results of calculation with one of the mechanisms turned off are shown for comparison. Linear purely Brownian growth (curve 3, $\tau_B = 3 \times 10^{-5} \, \mu s$, $\tau_H = 2 \, \mu s$) is obviously insufficient starting from 1 μs . The shear mechanism (line 4, $\tau_S = 0.08 \, \mu s$, $\tau_H = 2 \, \mu s$) provides exponential growth slow at the beginning and too fast at the end of the process. Note that as in [13], for this mechanism at $t \approx 3 \, \mu s$, there is agreement with experiment, but for any τ_S , it is possible at only one point.

According to gas-dynamic calculations [47], relation (21) with time $\tau_H \approx 2.8~\mu s$ holds quite well on the axis of a 20 mm diameter charge. The density decay on the axis is the slowest, and on average, the characteristic time of expansion $\tau_H = 2~\mu s$ seems quite realistic. The time τ_S also matches expectations. The velocity gradient Γ is essentially the inverse time of chemical reaction, and Γ^{-1} at a volume fraction of carbon $\phi \cong 0.1$ should be several times less than τ_S , i.e., about 20 ns. This seems to be a reasonable estimate for a sensitive substances such as BTF.

The time τ_B is taken to be approximately 15-fold longer than predicted by the above estimates $(\tau_B \approx 2 \times 10^{-6} \, \mu s)$. This discrepancy can be explained by the heterogeneity of the examined object. The synchrotron radiation scattering signal depends on the difference in density between the medium and par-

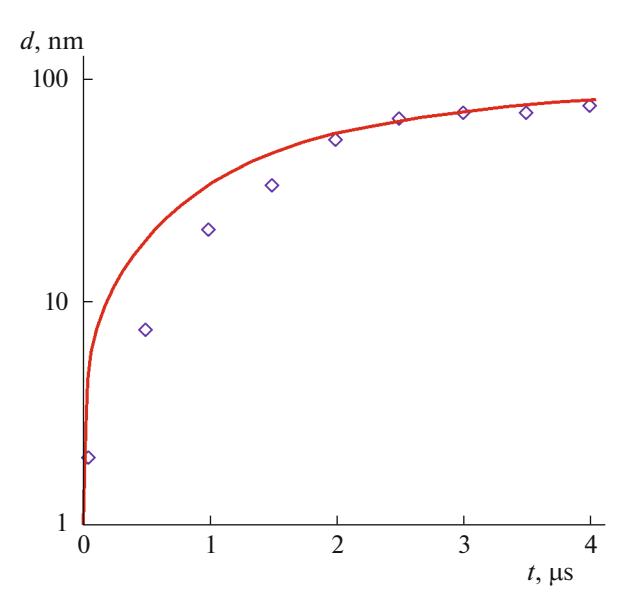


Fig. 4. Effect of accelerating the Brownian stage of growth.

ticles. During detonation, material expansion begins from the charge surface, where the density contrast is the highest. The outer regions, where the formation of relatively small particles can be expected, will be excessively represented in the scattered radiation, creating the impression of slow particle growth at the initial stage.

To roughly account for this effect, it is natural to abandon the exact reproduction of the initial stage of growth. Figure 4 shows the calculation results for $\tau_S = 0.11 \,\mu s$ and $\tau_H = 2.1 \,\mu s$, almost the same as in Fig. 3, but for significantly shorter $\tau_B = 4 \times 10^{-6} \,\mu s$. The calculation gives an approximately two-fold increase in size during the first microsecond, which presumably compensates for the initial underestimation of experimental data. Further, the same good agreement as in Fig. 3 is observed.

The value of τ_B selected for the calculation shown in Fig. 4 is already markedly closer to the expected value. The remaining twofold difference can be explained by the approximate nature of the estimate. Thus, the proposed growth model gives reasonable agreement with experiment. For the specified values of τ_B and τ_S , the mass M_* at which the shear mechanism becomes dominant is about 25000, and the time to reach this mass is close to 0.1 μ s.

In [18], the detonation of the explosive DNTF ($C_6N_8O_8$) was studied using the dynamic SAXS method. This explosive also does not contain hydrogen and has a high calculated detonation temperature (\approx 5200 K). Experiment [18] provides an opportunity for independent verification of the model (23). In particular, it is reported that the transition of the carbon component from the liquid to the solid phase takes about 0.2 µs. The particle size at the moment of the transition is estimated to be 9 nm at a temperature of \approx 4400 K. Considering that the diameter of the charges in this work was approximately three times smaller than in [15, 16] (6.35 and 20 mm, respectively), we can set the time $\tau_H = 0.7$ µs. Calculation by (23) with this time of expansion and the same times $\tau_B = 4 \times 10^{-6}$ µs and $\tau_S = 0.11$ µs as in Fig. 4 gave a characteristic size d = 8.8 nm at t = 0.2 µs, which should be considered an unexpectedly good agreement. The calculated size at t = 0.52 µs (maximum observation time in [18]) was about 12.6 nm, slightly larger than the average size of \approx 10 nm determined microscopically in material recovered after explosion. Nevertheless, the agreement here is also good.

PARTICLE GROWTH IN HYDROGEN-CONTAINING EXPLOSIVES

BTF, which does not contain hydrogen, is a bit of an anomaly. Much smaller particles are formed during the detonation of conventional hydrogen-containing explosives. Particle sizes of the order of several nanometers can be obtained by introducing the probability of particle merging upon contact. Such a

straightforward approach does not seem reasonable, which can be seen even from the extremely small size of this probability (e.g., in [48], it is estimated at 8×10^{-4}).

In practice, the probability of merging should at least depend on the particle sizes. A more reasonable model assumes a size limitation on the growth of compact particles [9, 10], in which small particles merge seamlessly like liquid drops even at a temperature lower than the standard (macroscopic) melting temperature. However, as the particle size increases, the particles gradually approach the solid state, which limits their growth. Without this limitation, one would expect approximately the same dynamics of sizes as in BTF, since velocity fluctuations and the characteristic scales of inhomogeneities cannot differ significantly. At the same time, the possibility of combining into fractal aggregates in which particles come into contact, mostly remaining individual. Aggregation in recovered explosion products was observed based on SAXS curves [9, 10] and microscopically [31]. In dynamic SAXS profiles, the aggregation effect is shown in [46]. For the above reasons, in conventional explosives it is sufficient to consider the Brownian stage of coagulation, which takes fractions of a microsecond.

It is important that loose aggregates with a fractal dimension D_f close to 2 occupy a much larger volume than the particles themselves. Therefore, very soon they begin to interfere with each other's growth due to the formation of a continuous network of carbon particles, a kind of aerogel. Note that carbon gel is formed even in a relatively rarefied medium such as the combustion products of acetylene at atmospheric pressure [49]. It has been shown [9, 10] that at a carbon volume fraction of $\phi \cong 0.1$ and particle radius a, a typical aggregate has a size of the order of $a/\phi = 10a$ and consists of $1/\phi^2 \cong 100$ particles. Such aggregates have been repeatedly found in the carbon residue recovered after explosion [31, 50].

Interestingly, almost the same aggregate size can be obtained from gas-dynamic considerations. Let us consider an aggregate of size L which is in a flow field with velocity gradient Γ (it is irrelevant whether the flow field arises from the general expansion or from hot-spot combustion). An individual particle of size a is subjected to the Stokes force of the order of $6\pi\mu a\Gamma L$, and the entire aggregate to the Stokes force $6\pi\mu a\Gamma L(L/a)^{D_f}\approx 6\pi\mu\Gamma L^3/a$. This force should break the bonding of this aggregate with the neighboring one. Neglecting the bonding strength, bonding rupture is prevented by the external pressure that presses one of the peripheral particles against a similar particle of the neighboring aggregate:

$$6\pi\mu\Gamma L^3/a \cong Pa^2, \quad \frac{L}{a} \cong \left(\frac{P}{6\pi\mu\Gamma}\right)^{1/3}.$$

At P=30 GPa, $\mu=0.014$ g/(cm s), and $1/\Gamma=20$ ns, we obtain $L/a\approx28$. The size will be slightly larger if the characteristic velocity gradient in the reaction zone is taken as Γ (it is approximately an order of magnitude smaller, and the size will increase by a factor of 2–2.5). Such a gradient can be expected on the axis of a cylindrical charge, but on the periphery, it is much larger, so that on average the value $L/a\approx10-20$ is quite likely.

In these calculations, it was assumed that the contact strength was small compared to the detonation pressure. Indeed, although small aggregates are quite stable, they can still be broken down into individual granules by standard laboratory techniques [51]. In addition, it was assumed that viscous friction acted on all particles constituting the aggregate. This is justified since the flow is constrained: the gas is forced to filter through the carbon aerogel network. An isolated aggregate has lower hydrodynamic resistance since mainly its outside is subjected to the flow, and the resistance is proportional to its size [52], and not to the number of particles. This regime is possible in the case of significant expansion of detonation products, where small initial aggregates can merge into larger ones.

In the case of aerogel formation, the subsequent growth of particles occurs mainly due to the expansion of the medium, leading to rupture of the gel in the weakest places. This can lead to new contacts between aggregates, resulting in particle enlargement, though with low probability. This mechanism seems more natural than the exchange of fragments proposed in [19]. Paradoxically, gas-dynamic expansion slowing down unlimited coagulation promotes limited coagulation. This is apparently responsible for the extremely slow growth of compact particles [46] over several microseconds. The late growth effect is also observed in practice: in detonation synthesis using charges weighing tens and even hundreds of kilograms, the particle size reliably increases [53]. In this connection, we can mention the hypothesis put forward by Anisichkin that solid-phase growth is due to the resonance of optical and acoustic vibrations during particle collisions [54], as well as the less specific ideas [30] about the gradual enlargement of the particles in a fractal aggregate.

Table 1

T, K		Reference
BTF	RDX	Reference
4590	3220	[56]
4059	2587	[57]
5600	4074	[58]
4917	3488	[59]
5693	3818	[55]
5570	4140	[60]
4200	3700	[61]

During the detonation of BTF, the aerogel stage is not reached, since initially (during the first $1-2\,\mu s$) compact particles reaching tens of nanometers are formed. Later, as the temperature decreases, these particles lose the ability to merge as liquid drops and begin to form more or less porous but not fractal conglomerates – lumps hundreds of nanometers in size. Such structures are observed microscopically. However, at this stage, gas-dynamic expansion, leading to an increase in the distance between particles and preventing gel formation, is already noticeable. This justifies the long coagulation approximation used in calculations where no distinction was made between the stages of compact particles and lumps.

NATURE OF THE PARTICLE SIZE DIFFERENCE

The formation of abnormally large particles during the detonation of BTF was associated with elevated temperature, i.e., with growth predominantly in the liquid phase, or with the absence of hydrogen and/or hydrogen-containing groups that presumably occupy the surface of particles and slowing their growth.

We first discuss the temperature factor. Historically, BTF was assumed to have an unusually high detonation temperature. In some calculations, it reached $\approx 5700 \text{ K}$ [55], against $\approx 3800 \text{ K}$ in dense RDX. Other papers reported somewhat lower values. Table 1 shows the calculated temperatures in the Chapman–Jouguet state for BTF with a density of 1.859 g/cm^3 and RDX with a density of 1.8 g/cm^3 .

Obviously, temperature is a quantity which is the least reliably determined by calculation. Experimental measurements of the detonation temperature of solid explosives are generally few in number. In particular, data for BTF are given only in [62]. Although the measured temperature of \approx 4100 K was higher than the temperature obtained by the same authors in RDX (\approx 3740 K), but this difference is significantly smaller than expected from most calculations.

The concept of high-temperature liquid-phase coagulation suggests the validity of most early estimates of temperature during the detonation of BTF. Perhaps the data of [61, 62] should be revised upward. Note that the temperature decrease over time in BTF [62] was significantly slower than in RDX and HMX [63], which speaks in favor of the temperature factor.

It is known that the surface of ultradispersed detonation diamonds is covered with various groups of foreign atoms, and almost each surface carbon atom is bonded to a heteroatom. Hydrogen atoms are the most numerous among these surface contaminants [50]. It is reasonable to expect that such contaminants occur already during the formation of particles and that in conventional hydrogen-containing explosives, the OH, $\rm H_2O$, and similar groups can interfere with coagulation. Accordingly, in BTF, this hindrance is less significant. The data [15, 16] show that the initial rate of particle growth in BTF is much higher than in the 50/50 TNT/RDX composition. At the same time, the parameters of the medium do not differ significantly (except for the absence of hydrogen in BTF and the temperature difference discussed above), so that the Brownian stage of coagulation should formally proceed in a similar way.

Thus, the absence of hydrogen-containing contaminants should be recognized as one of the reasons for the anomaly of BTF. However, the main factor seems to be the high detonation temperature. The important role of temperature is confirmed by the morphology of large clots (see the micrographs of recovered products in [42]); ideal balls obtained by detonation of DNTF are especially characteristic [18]. Finally, we note the work [64], in which marked increase in particle size by increasing the synthesis temperature was achieved.

It is also necessary to take into account important details of the particle collision process noted in molecular dynamics simulations [32, 33]: the presence of a quasi-liquid layer on the particle surface, the exothermicity of cluster coagulation and the pressure waves generated by the coagulation, whose amplitude reaches 30 GPa, i.e., has the same order as the detonation pressure. All these phenomena can significantly expand the coagulation region and, under favorable conditions in BTF detonation, lead to the formation of abnormally large particles.

CONCLUSIONS

The calculation of the growth curve presented in Fig. 4 gave reasonable agreement with experiment, and the constants used agree with a priori estimates with acceptable accuracy. The roughness of the model corresponds to the level of accuracy of the experimental data and their interpretation. As already mentioned above, an important factor is the dynamics of the density contrast between the gas and particles. The final particle sizes are determined fairly accurately (and confirmed by microscopic measurements of condensed products), whereas at the initial stages, the closeness of the gas and particle densities can introduce strong distortions, creating the impression of slow growth. This effect probably manifests itself as a noticeable slowdown in the growth of particles and clusters with increasing size of the charge [46]. Careful modeling of the expansion, combined with small-angle scattering calculations, will make it possible to clarify the dynamics of sizes and provide a more detailed understanding of particle growth.

The kinetics of carbon coagulation during detonation was first discussed in detail in the paper by Shaw and Johnson [1]. In paying tribute to this important work, it should be noted that with the accumulation of new data, the approach of these authors looks too simplified. In particular, the explanation of the non-ideality effects in the detonation of carbon-rich explosives such as TNT and TATB by the unlimited diffusion growth of carbon particles should at least be clarified in light of available information. Due to the low detonation temperature and the presence of hydrogen-containing groups, the typical particle size in these explosives is a few nanometers, and the particle growth is stopped at an early stage by the formation of fractal gel. Further release of surface energy is possible only due to the destruction of the gel during expansion of the medium. It is this complex kinetics that may be responsible for the nonideality of the detonation of TNT and TATB (which manifests itself, in particular, in the significant scatter of experimental data for these explosive). In contrast, practically unhindered growth limited only by gas-dynamic expansion is observed in BTF, which is one of the most striking examples of an ideal explosive.

FUNDING

This work was carried out within the framework of the state assignment of the Institute of Hydrodynamics, Siberian Branch, Russian Academy of Sciences (project no. 2.3.1.2.5, research topic code: FWGG-2021-0004).

CONFLICT OF INTEREST

The author of this work declares that he has no conflicts of interest.

NOTE ON PROOFREEDING

While preparing the proofs, the author familiarized himself with the article [65], which has provided experimental evidence supporting some of the concepts outlined in this paper.

REFERENCES

- Shaw, M.S. and Johnson, J.D., Carbon clustering in detonations, *J. Appl. Phys.*, 1987, vol. 62, no. 5, pp. 2080–2085. https://doi.org/10.1063/1.339554
- Viecelli, J.A. and Ree, F.H., Carbon clustering kinetics in detonation wave propagation, *J. Appl. Phys.*, 1999, vol. 86, no. 1, pp. 237–248. https://doi.org/10.1063/1.370722
- 3. Volkov, K.V., Danilenko, V.V., and Elin, V.I., Synthesis of diamond from the carbon in the detonation products of explosives, *Combust., Explos., Shock Waves*, 1990, vol. 26, no. 3, pp. 366–368. https://doi.org/10.1007/bf00751383
- 4. Danilenko, V.V., *Sintez i spekanie almaza vzryvom* (Synthesis and Sintering of Diamond by Explosion), Moscow: Energoatomizdat, 2003.

- Staver, A.M., Ershov, A.P., and Lyamkin, A.I., Study of detonations in condensed explosives by conduction methods, *Combust., Explos., Shock Waves*, 1984, vol. 20, no. 3, pp. 320–323. https://doi.org/10.1007/bf00782918
- 6. Staver, A.M., Gubareva, N.V., Lyamkin, A.I., and Petrov, E.A., Ultrafine diamond powders made by the use of explosion energy, *Combust., Explos., Shock Waves*, 1984, vol. 20, no. 5, pp. 567–570.
- Lyamkin, A.I., Petrov, E.A., Ershov, A.P., Sakovich, G.V., Staver, A.M., and Titov, V.M., Production of diamond from explosives, *Sov. Phys. Dokl.*, 1988, vol. 33, no. 3, pp. 705–706. https://doi.org/10.1037/025903
- Greiner, N.R., Phillips, D.S., Johnson, J.D., and Volk, F., Diamonds in detonation soot, *Nature*, 1988, vol. 333, no. 6172, pp. 440–442. https://doi.org/10.1038/333440a0
- 9. Ershov, A.P., Kupershtokh, A.L., and Kolomiichuk, V.N., Detonation-produced fractal structures, *Tech. Phys. Lett.*, 1990, vol. 16, no. 3, pp. 42–46.
- 10. Ershov, A.P. and Kupershtokh, A.L., Fractal structure formation in explosion, *Combust., Explos., Shock Waves*, 1991, vol. 27, no. 2, pp. 231–236.
- 11. Danilenko, V.V., Specific features of synthesis of detonation nanodiamonds, *Combust., Explos., Shock Waves*, 2005, vol. 41, no. 5, pp. 577–588. https://doi.org/10.1007/s10573-005-0072-5
- 12. Mal'kov, I.Yu., Filatov, L.I., Titov, V.M., Litvinov, B.V., Chuvilin, A.L., and Teslenko, T.S., Formation of diamond from the liquid phase of carbon, *Combust., Explos., Shock Waves*, 1993, vol. 29, no. 4, pp. 542–544. https://doi.org/10.1007/bf00782983
- 13. Mal'kov, I.Yu., Carbon coagulation in a nonstationary detonation-product flow, *Combust., Explos., Shock Waves*, 1994, vol. 30, no. 5, pp. 720–722.
- Aleshaev, A.N., Zubkov, P.I., Kulipanov, G.N., Luk'yanchikov, L.A., Lyakhov, N.Z., Mishnev, S.I., Ten, K.A., Titov, V.M., Tolochko, B.P., Fedotov, M.G., and Sheromov, M.A., Application of synchrotron radiation for studying detonation and shock-wave processes, *Combust., Explos., Shock Waves*, 2001, vol. 37, no. 5, pp. 585–593. https://doi.org/10.1023/a:1012353406187
- Titov, V.M., Pruuél, E.R., Ten, K.A., Luk'yanchikov, L.A., Merzhievskii, L.A., Tolochko, B.P., Zhulanov, V.V., and Shekhtman, L.I., Experience of using synchrotron radiation for studying detonation processes, *Combust., Explos., Shock Waves*, 2011, vol. 47, no. 6, pp. 615–626. https://doi.org/10.1134/s0010508211060013
- Ten, K.A., Titov, V.M., Pruuel, E.R., Kashkarov, A.O., Tolochko, B.P., Aminov, Yu.A., Loboyko, B.G., Muzyrya, A.K., and Smirnov, E.B., Carbon condensation in detonation of high explosives, *Proc. 15th International Detonation Symposium*, 2014, pp. 369–374.
- Bagge-Hansen, M., Lauderbach, L., Hodgin, R., Bastea, S., Fried, L., Jones, A., van Buuren, T., Hansen, D., Benterou, J., May, C., Graber, T., Jensen, B.J., Ilavsky, J., and Willey, T.M., Measurement of carbon condensates using small-angle X-ray scattering during detonation of the high explosive hexanitrostilbene, *J. Appl. Phys.*, 2015, vol. 117, no. 24, p. 245902. https://doi.org/10.1063/1.4922866
- Bagge-Hansen, M., Bastea, S., Hammons, J.A., Nielsen, M.H., Lauderbach, L.M., Hodgin, R.L., Pagoria, P., May, C., Aloni, S., Jones, A., Shaw, W.L., Bukovsky, E.V., Sinclair, N., Gustavsen, R.L., Watkins, E.B., Jensen, B.J., Dattelbaum, D.M., Firestone, M.A., Huber, R.C., Ringstrand, B.S., Lee, J.R.I., van Buuren, T., Fried, L.E., and Willey, T.M., Detonation synthesis of carbon nano-onions via liquid carbon condensation, *Nat. Commun.*, 2019, vol. 10, no. 1, p. 3819. https://doi.org/10.1038/s41467-019-11666-z
- 19. Purohit, A. and Velizhanin, K.A., Kinetics of carbon condensation in detonation of high explosives: First-order phase transition theory perspective, *J. Chem. Phys.*, 2021, vol. 155, no. 16, p. 164302. https://doi.org/10.1063/5.0064735
- von Smoluchowski, M.V., Versuch einer mathematischen theorie der koagulationskinetik kolloider lösungen, Z. Phys. Chem., 1917, vol. 92, no. 1, pp. 129–168. https://doi.org/10.1515/zpch-1918-9209
- 21. Chandrasekhar, S., Stochastic problems in physics and astronomy, *Rev. Mod. Phys.*, 1943, vol. 15, no. 1, pp. 1–89. https://doi.org/10.1103/revmodphys.15.1
- 22. Hidy, G.M., On the theory of the coagulation of noninteracting particles in Brownian motion, *J. Colloid Sci.*, 1965, vol. 20, no. 2, pp. 123–144. https://doi.org/10.1016/0095-8522(65)90003-6
- 23. Friedlander, S.K. and Wang, C.S., The self-preserving particle size distribution for coagulation by Brownian motion, *J. Colloid Interface Sci.*, 1966, vol. 22, no. 2, pp. 126–132. https://doi.org/10.1016/0021-9797(66)90073-7

- 24. Bastea, S., Transport properties of fluid mixtures at high pressures and temperatures. Application to the detonation products of HMX, *Proc. 12th International Detonation Symposium*, San Diego, CA, 2002, pp. 576–583.
- 25. Kopyshev, V.P., Medvedev, A.B., and Khrustalev, V.V., Model estimation of the viscosity of explosion products of condensed explosives, *Combust., Explos., Shock Waves*, 2004, vol. 40, no. 2, pp. 200–208. https://doi.org/10.1023/b:cesw.0000020142.45935.a6
- 26. Chevrot, G., Sollier, A., and Pineau, N., Molecular dynamics and kinetic study of carbon coagulation in the release wave of detonation products, *J. Chem. Phys.*, 2012, vol. 136, no. 8, p. 084506. https://doi.org/10.1063/1.3686750
- 27. Ornellas, D.L., Heat and products of detonation of cyclotetramethylenetetranitramine, 2,4,6-trinitrotoluene, nitromethane, and bis[2,2-dinitro-2-fluoroethyl] formal, *J. Phys. Chem.*, 1968, vol. 72, no. 7, pp. 2390–2394. https://doi.org/10.1021/j100853a019
- 28. Ornellas, D.L., The heat and products of detonation in a calorimeter of CNO, HNO, CHNF, CHNOF, and CHNOSi explosives, *Combust. Flame*, 1974, vol. 23, no. 1, pp. 37–46. https://doi.org/10.1016/s0010-2180(74)80025-8
- 29. Titov, V.M., Anisichkin, V.F., and Mal'kov, I.Yu., Synthesis of ultradispersed diamond in detonation waves, *Combust., Explos., Shock Waves*, 1989, vol. 25, no. 3, pp. 372–379.
- Velizhanin, K.A. and Watkins, E.B., Modeling carbon condensation in detonation of high explosives: A tale of two approximations, *AIP Conf. Proc.*, 2023, vol. 2844, no. 1, p. 290013. https://doi.org/10.1063/12.0020373
- 31. Sakovich, G.V., Gubarevich, V.D., Badaev, F.Z., Brylyakov, P.M., and Besedina, O.A., Aggregation of detonation nanodiamonds, *Dokl. Akad. Nauk SSSR*, 1990, vol. 310, no. 2, pp. 402–404.
- 32. Kupershtokh, A.L., Ershov, A.P., and Medvedev, D.A., Coagulation of carbon clusters in detonation front, *AIP Conf. Proc.*, 1996, vol. 370, no. 1, pp. 393–396. https://doi.org/10.1063/1.50804
- 33. Kupershtokh, A.L., Ershov, A.P., and Medvedev, D.A., Model for the coagulation of carbon clusters at high densities and temperatures, *Combust., Explos., Shock Waves*, 1998, vol. 34, no. 4, pp. 460–466. https://doi.org/10.1007/bf02675616
- 34. Hammons, J.A., Nielsen, M.H., Bagge-Hansen, M., Bastea, S., Shaw, W.L., Lee, J.R.I., Ilavsky, J., Sinclair, N., Fezzaa, K., Lauderbach, L.M., Hodgin, R.L., Orlikowski, D.A., Fried, L.E., and Willey, T.M., Resolving detonation nanodiamond size evolution and morphology at sub-microsecond timescales during high-explosive detonations, *J. Phys. Chem. C*, 2019, vol. 123, no. 31, pp. 19153–19164. https://doi.org/10.1021/acs.jpcc.9b02692
- 35. Saffman, P.G. and Turner, J.S., On the collision of drops in turbulent clouds, *J. Fluid Mech.*, 1956, vol. 1, no. 1, pp. 16–30. https://doi.org/10.1017/s0022112056000020
- 36. Saffman, P.G. and Turner, J.S., Corrigendum on the collision of drops in turbulent clouds, *J. Fluid Mech.*, 1988, vol. 196, p. 599. https://doi.org/10.1017/S002211208800285X
- 37. Safronov, V.S., A particular solution of the coagulation equation, *Dokl. Akad. Nauk SSSR*, 1962, vol. 147, no. 1, pp. 64–67.
- 38. Golovin, A.M., On the solution of the coagulation equation for raindrops taking into account condensation, *Dokl. Akad. Nauk SSSR*, 1963, no. 8, p. 191.
- 39. Lushnikov, A.A., Evolution of coagulating systems, *J. Colloid Interface Sci.*, 1973, vol. 45, no. 3, pp. 549–556. https://doi.org/10.1016/0021-9797(73)90171-9
- 40. Lushnikov, A.A. and Tokar', Ya.I., Gamma-approximation for asymptotic spectra in coagulating systems, *Kolloidn. Zh.*, 1980, vol. 42, no. 3, pp. 475–479.
- 41. Dimotakis, P.E., The mixing transition in turbulent flows, *J. Fluid Mech.*, 2000, vol. 409, pp. 69–98. https://doi.org/10.1017/s0022112099007946
- 42. Satonkina, N., Ershov, A., Kashkarov, A., Mikhaylov, A., Pruuel, E., Rubtsov, I., Spirin, I., and Titova, V., Electrical conductivity distribution in detonating benzotrifuroxane, *Sci. Rep.*, 2018, vol. 8, no. 1, p. 9635. https://doi.org/10.1038/s41598-018-28028-2
- 43. Williams, M.M.R., A unified theory of aerosol coagulation, *J. Phys. D: Appl. Phys.*, 1988, vol. 21, no. 6, pp. 875–886. https://doi.org/10.1088/0022-3727/21/6/004
- 44. Avramenko, M.I., *O k-ε modeli turbulentnosti* (On the *k–ε* Model of Turbulence), Snezhinsk: RFYaTs-VNIITF, 2010, 2nd ed.
- 45. Ershov, A.P., Simulation of synchrotron diagnostics of explosion, *Tech. Phys. Lett.*, 2001, vol. 27, no. 19, pp. 90–94.
- 46. Rubtsov, I.A., Two-stage carbon condensation model during detonation of high explosives, *Sib. Fiz. Zh.*, 2022, vol. 17, no. 2, pp. 48–55. https://doi.org/10.25205/2541-9447-2022-17-2-48-55

- Rubtsov, I.A., Ten, K.A., Pruuel, E.R., Kashkarov, A.O., Kremenko, S.I., Voronin, M.S., Shekhtman, L.I., Zhulanov, V.V., and Tolochko, B.P., Methods to restore the dynamics of carbon condensation during the detonation of high explosives, *J. Phys.: Conf. Ser.*, 2019, vol. 1147, p. 012038. https://doi.org/10.1088/1742-6596/1147/1/012038
- 48. Bastea, S., Aggregation kinetics of detonation nanocarbon, *Appl. Phys. Lett.*, 2012, vol. 100, no. 21, p. 214106. https://doi.org/10.1063/1.4722783
- 49. Sorensen, C.M., Hageman, W.B., Rush, T.J., Huang, H., and Oh, C., Aerogelation in a flame soot aerosol, *Phys. Rev. Lett.*, 1998, vol. 80, no. 8, pp. 1782–1785. https://doi.org/10.1103/physrevlett.80.1782
- 50. Dolmatov, V.Yu., Ultradispersed detonation-synthesized diamonds: Properties and applications, *Russ. Chem. Rev.*, 2001, vol. 70, no. 7, pp. 607–626.
- 51. Krüger, A., Kataoka, F., Ozawa, M., Fujino, T., Suzuki, Y., Aleksenskii, A.E., Vul', A.Ya., and Ōsawa, E., Unusually tight aggregation in detonation nanodiamond: Identification and disintegration, *Carbon*, 2005, vol. 43, no. 8, pp. 1722–1730. https://doi.org/10.1016/j.carbon.2005.02.020
- 52. Sorensen, C.M., The mobility of fractal aggregates: A review, *Aerosol Sci. Technol.*, 2011, vol. 45, no. 7, pp. 765–779. https://doi.org/10.1080/02786826.2011.560909
- 53. Vyskubenko, B.A., Danilenko, V.V., Lin, E.E., Mazanov, V.A., and Serova, T.V., Effect of scaling on size and yield of diamonds in detonation synthesis, *Fiz. Goreniya Vzryva*, 1992, vol. 28, no. 2, pp. 108–109.
- 54. Anisichkin, V.F., The phenomenon of resonant solid-phase coalescence of small diamond particles in explosion products, *Khim. Fiz.*, 1993, vol. 12, no. 5, pp. 605–608.
- 55. Kondrikov, B.N. and Sumin, A.I., Equation of state for gases at high pressure, *Combust., Explos., Shock Waves*, 1987, vol. 23, no. 1, pp. 105–113.
- 56. Finger, M., Lee, E., and Helm, F.H., The effect of elemental composition on the detonation behavior of explosives, *Proc. 6th Symposium (International) on Detonation*, Virginia, 1976, pp. 710–722.
- 57. Mader, C.L., Numerical Modeling of Detonations, Berkeley: Univ. California Press, 1979.
- 58. Chirat, R. and Baute, J., An extensive application of WCA4 equation of state for explosives, *Proc. 8th Symposium (International) on Detonation*, 1985, pp. 751–761.
- 59. Tanaka, K., Detonation properties of high explosives calculated by revised Kihara—Hikita equation of state, *Proc. 8th Symposium (International) on Detonation*, 1985, pp. 548–557.
- 60. Hobbs, D.B. and Baer, M.R., Calibrating the BKW-EOS with a large product species data base and measured C-J properties, *Proc. 10th International Detonation Symposium*, Office of Naval Research, 1993, pp. 409–418.
- 61. Pruuel, E.R., High-speed X-ray tomography and the equation of state of condensed explosive detonation products, *Doctoral (Phys.-Math.) Dissertation*, Novosibirsk: Inst. Hydrodyn., Sib. Branch, Russ. Acad. Sci., 2022.
- Dolgoborodov, A.Yu., Brajnikov, M.A., Makhov, M.N., Safronov, N.E., and Kirilenko, V.G., Detonation parameters of pressed charges of benzotrifuroxane, *Combust., Explos., Shock Waves*, 2013, vol. 49, no. 6, pp. 723

 –730. https://doi.org/10.1134/s0010508213060129
- 63. Gogulya, M.F. and Brazhnikov, M.A., Temperature of condensed explosive detonation products. I. Solid explosives, *Khim. Fiz.*, 1994, vol. 13, no. 1, pp. 52–63.
- 64. Anisichkin, V.F., Dolgushin, D.S., and Petrov, E.A., The effect of temperature on the growth of ultradispersed diamonds at a detonation front, *Combust., Explos., Shock Waves*, 1995, vol. 31, no. 1, pp. 109–112.
- 65. Hammons, J.A., Nielsen, M.H., Bagge-Hansen, M., Bastea, S., May, C., Shaw, W.L., Martin, A., Li, Y., Sinclair, N., Lauderbach, L.M., Hodgin, R.L., Orlikowski, D.A., Fried, L.E., and Willey, T.M., Submicrosecond aggregation during detonation synthesis of nanodiamond, *J. Phys. Chem. Lett.*, 2021, vol. 12, no. 22, pp. 5286–5293.

https://doi.org/10.1021/acs.jpclett.1c01209

Publisher's Note. Pleiades Publishing remains neutral with regard to jurisdictional claims in published maps and institutional affiliations.

AI tools may have been used in the translation or editing of this article.